NeuroImage 189 (2019) 141–149

Contents lists available at ScienceDirect

NeuroImage

journal homepage: www.elsevier.com/locate/neuroimage

# Customized head molds reduce motion during resting state fMRI scans

Jonathan D. Power *, Benjamin M. Silver, Melanie R. Silverman, Eliana L. Ajodan, Dienke J. Bos, Rebecca M. Jones

*Sackler Institute for Developmental Psychobiology, Department of Psychiatry, Weill Cornell Medicine, 1300 York Avenue, Box 140, New York, NY, 10065, USA*

A B S T R A C T

Head motion causes artifacts in functional magnetic resonance imaging (fMRI) scans, a problem especially relevant for task-free resting state paradigms and for developmental, aging, and clinical populations. In a cohort spanning 7–28 years old (mean age 15) we produced customized head-anatomy-specific Styrofoam molds for each subject that inserted into an MRI head coil. We scanned these subjects under two conditions: using our standard procedure of packing the head coil with foam padding about the head to reduce head motion, and using the customized molds to reduce head motion. In 12 of 13 subjects, the molds reduced head motion throughout the scan and reduced the fraction of a scan with substantial motion (i.e., volumes with motion notably above baseline levels of motion). Motion was reduced in all 6 head position estimates, especially in rotational, left-right, and superior-inferior directions. Motion was reduced throughout the full age range studied, including children, adolescents, and young adults. In terms of the fMRI data itself, quality indices improved with the head mold on, scrubbing analyses detected less distance-dependent artifact in scans with the head mold on, and distant-dependent artifact was less evident in both the entire scan and also during only low-motion volumes. Subjects found the molds comfortable. Head molds are thus effective tools for reducing head motion, and motion artifacts, during fMRI scans.

## 1. Introduction

Head motion is a problem in functional magnetic resonance imaging (fMRI) because it causes large artifacts in signals (Friston et al., 1996). In task fMRI, such artifacts can be averaged away via the task design (unless motion is related to the task design (Barch et al., 1999; Bullmore et al., 1999; Epstein et al., 2007)). However, in "functional connectivity" fMRI studies, where signal covariance over time is the feature of interest, no such averaging can occur. Further, motion introduces colored covariance into data, for spatially focal motion artifacts preferentially elevate covariance between nearby signals relative to distant signals (Power et al., 2012; Satterthwaite et al., 2012; Van Dijk et al., 2012).

Since the recognition of the spurious but systematic influence of motion on resting state covariance, a substantial amount of effort has been devoted to developing post-hoc techniques to characterize and remove motion-related signals in fMRI (and other) scans (Baum et al., 2018; Bright and Murphy, 2013; Ciric et al., 2017; Fair et al., 2012; Kundu et al., 2013; Patel et al., 2014; Power, 2017; Power et al., 2014, 2017a, 2017b, 2018; Pruim et al., 2015; Salimi-Khorshidi et al., 2014; Satterthwaite et al., 2013, 2017; Savalia et al., 2017; Yan et al., 2013). Some effort has also been directed at developing T2*-weighted sequences that correct for motion during acquisition (reviewed in (Zaitsev et al., 2017)), though these approaches are not in wide use. Curiously, relatively little effort has been directed at preventing motion from occurring in the first place.

Motion can be reduced either via behavioral interventions (i.e., training the subject to be still) or by physically preventing the head from moving. In pediatric populations, which are the subject of this report and in which motion is a major problem, it is common practice to acclimate children to a scanning environment via a mock scanner (Barnea-Goraly et al., 2014; de Bie et al., 2010; Epstein et al., 2007; Nordahl et al., 2016), often with feedback about head motion from cameras intended to train the child to move less. Increasingly, it is possible to monitor motion during actual fMRI scanning, and feedback can reduce motion in this setting (Dosenbach et al., 2017; Greene et al., 2018). These behavioral techniques are variably effective across subjects, and a potential downside is that they introduce attention to staying still to the task-free resting state (which is classically performed with minimal instruction to subjects).

An alternative approach is to physically restrain the head from moving. With non-human animals, head posting can completely immobilize the head. With humans, it is common practice to pack MRI head coils with foam pads to mildly restrain the head (this approach forms our control "mold OFF" condition below). Some groups use thermoplastic masks over the nose and brow fixed to the head coil, but these masks also only mildly restrain the head. Some groups have used small head coils for scanning infants but these still permit motion within the head coil (Deen et al., 2017). Bite bars can be used, but many subjects find these

* Corresponding author.
*E-mail addresses:* jdp9009@nyp.org (J.D. Power), bes2037@med.cornell.edu (B.M. Silver), melaniesilverman22@gmail.com (M.R. Silverman), eajodan@gmail.com (E.L. Ajodan), D.J.Bos-2@umcutrecht.nl (D.J. Bos), rej2004@med.cornell.edu (R.M. Jones).

https://doi.org/10.1016/j.neuroimage.2019.01.016
Received 17 October 2018; Received in revised form 13 December 2018; Accepted 7 January 2019
Available online 9 January 2019

uncomfortable, and they can provoke salivation and swallowing, which causes head motion. The advent of "3-D" printing and milling over the last decade has made it possible to consider another approach: to create a customized mold of a subject's head that inserts into a head coil. Such molds could be both comfortable and effective at preventing head motion.

In this paper we document how customized head molds reduce head motion, and motion artifacts, during resting state fMRI scans. Our head molds were milled by a commercial company and are made of Styrofoam. We interacted with the company to trouble-shoot child-specific issues that arose, and we report problems we encountered and their eventual fixes. The procedure of obtaining a head mold consisted of using a hand-held optical scanner to scan the head and then waiting a few days for a mold to be produced and shipped; the costs were reasonable relative to the cost of subject recruitment and scanning. We scanned 13 subjects 4 times each, acquiring two scans without a head mold and two scans with a head mold in single sessions of scanning. In 12 of 13 subjects, the molds significantly reduced motion and significantly increased the fraction of a scan without substantial motion (i.e., reduced the number of volumes with notably above-baseline amounts of motion). Further, the fMRI scans obtained with the head molds on demonstrate improved quality measures and reduced motion artifact relative to scans obtained using the standard foam packing technique.

## 2. Methods

### 2.1. Subject recruitment

14 healthy control subjects (12 males, 2 females; ages $15 \pm 5$ years old) were recruited without contraindication to MRI scanning. All subjects or caregivers reported no past or current psychiatric or neurological diagnoses. One subject did not complete fMRI scanning and was excluded from analyses. Informed written consent (assent from minors, consent from caregivers) was obtained from all participants and the study protocol was approved by the Weill Cornell Medicine Institutional Review Board.

### 2.2. Head mold production

Head molds were produced by the Caseforge company (https://caseforge.co), which provided us with a hand-held camera. Participants visited the lab twice. On the first visit, subjects were scanned with the Caseforge camera from 360° while wearing a swim cap. The swim cap was used since hair interferes with capturing the shape of the subject's head. The camera's image was digitally sent to the Caseforge company, which produced and shipped a customized Styrofoam mold within days. The head mold has 2 pieces, a front and a back, and is open in the face. One of our subjects and their family gave permission to show images of the mold, seen in Figure S1. Some children found it fun and/or comforting to decorate their head molds with MRI-safe markers. In addition, on the first visit, participants 17 years old and younger were acclimated to the MRI environment in a mock MRI scanner, and were trained to keep their head still via feedback following our usual procedures (similar to those described in (Casey et al., 2018)).

### 2.3. MRI scanning

Subjects returned for a second visit to undergo MRI scans. In scans without the head mold, foam pads were placed in the head coil to constrain head motion per our standard practices. In scans with the head mold, the back piece of the mold was placed in head coil, the subject lay back and fit their head into the mold, and the front piece was then placed. Since the head mold fit the face snugly, no additional padding was needed (or could be placed). Thus, our approach was to compare our typical motion-constraining approach of stuffing the head coil with pads ("mold OFF" condition) to filling the coil with a customized Styrofoam mold of the head ("mold ON" condition). We used earbuds that fit through ear holes so that subjects could easily communicate with the experimenter. Each subject completed 4 fMRI runs of 4.8 min duration, two runs with and two runs without the head mold. The first 5 subjects recruited underwent an AABB scan order (A = mold OFF; B = mold ON), and the remaining 8 subjects underwent counterbalanced ABAB or BABA orders.

Subjects were scanned in a Siemens Magnetom Prisma 3T scanner at the Citigroup Biomedical Imaging Center of Weill Cornell's medical campus using a Siemens 32-channel head coil. Functional images were acquired using the ABCD multi-band sequence (Casey et al., 2018), which has multi-band factor of 6. Functional images were acquired using T2*-weighted echo-planar sequences covering the full brain (TR = 800 ms, TE = 30 ms, FOV = 216 mm, flip angle = 49°, 2.4 mm isotropic, 66 slices), with 360 volumes acquired per run (total 4.8 min). For the resting state scans, subjects were asked to lie still and to fixate a white crosshair on a black screen, and received no other instruction. Respiratory bellows records were collected on some subjects using the Siemens abdominal belt, though most of these records were later discovered to have been misacquired. A high-resolution T1-weighted image (MP-RAGE) was obtained with TR = 2400 ms, TE = 2.12 ms, FOV = 256 mm, and 1 mm isotropic resolution.

### 2.4. Data processing: motion estimation

Head position during the resting state runs was estimated using the AFNI tool 3dvolreg, yielding 3 translation and 3 rotation estimates at each volume. The position parameters were used to form Framewise Displacement (FD) measures using established conventions (Power et al., 2012, 2015). Briefly, all six head position parameters were differentiated in time by backwards differences, angular changes were converted to arc displacement at 50 mm radius, and FD was calculated as the sum of the absolute values of the differentiated parameters. By convention, FD = 0 at the first volume.

Each subject had two runs with a mold and two runs without a mold. The mean and median FD values over each run were calculated, and the average was calculated in each subject for runs with and without the mold. These individual and average values are plotted in Fig. 2, and the average values were entered into paired t-tests. High-motion volumes were defined as those with FD > 0.30 mm, the fraction of volumes that were high-motion was calculated for each run, and these statistics were treated in a similar manner as the above statistics. To assess the parts of the scan without substantial motion, mean and median FD were also recalculated and re-compared without including high motion volumes, shown in Fig. 3.

To capture absolute displacement of the head in each realignment parameter, the absolute difference from the first volume was calculated. To capture absolute motion in each realignment parameter, the position parameter was differentiated by backwards differences, and the absolute value was taken. These values were compared (via run means, medians, and standard deviations) in the same way as the above statistics.

### 2.5. Data processing: fMRI signal assessment

fMRI scans were transformed into the Talairach TT-N27 atlas space by concatenating motion correction (AFNI's 3dvolreg), T2*-weighted to MP-RAGE (AFNI's align_epi_anat.py), and MP-RAGE to atlas transformations (AFNI's 3DAllineate) into a single applied transformation, with resampling to a 3 mm isotropic grid. Each initial transformation was computed separately, following procedures documented in (Power et al., 2017a, 2017b, 2018). FreeSurfer 5.3 was used to segment the T1-weighted image as in (Power, 2017; Power et al., 2017a, 2017b), and a whole-brain spatial mask from this segmentation was used to compute DVARS. All images were visually examined for goodness of registration prior to use.

DVARS is a data quality measure that indexes the rate of signal change

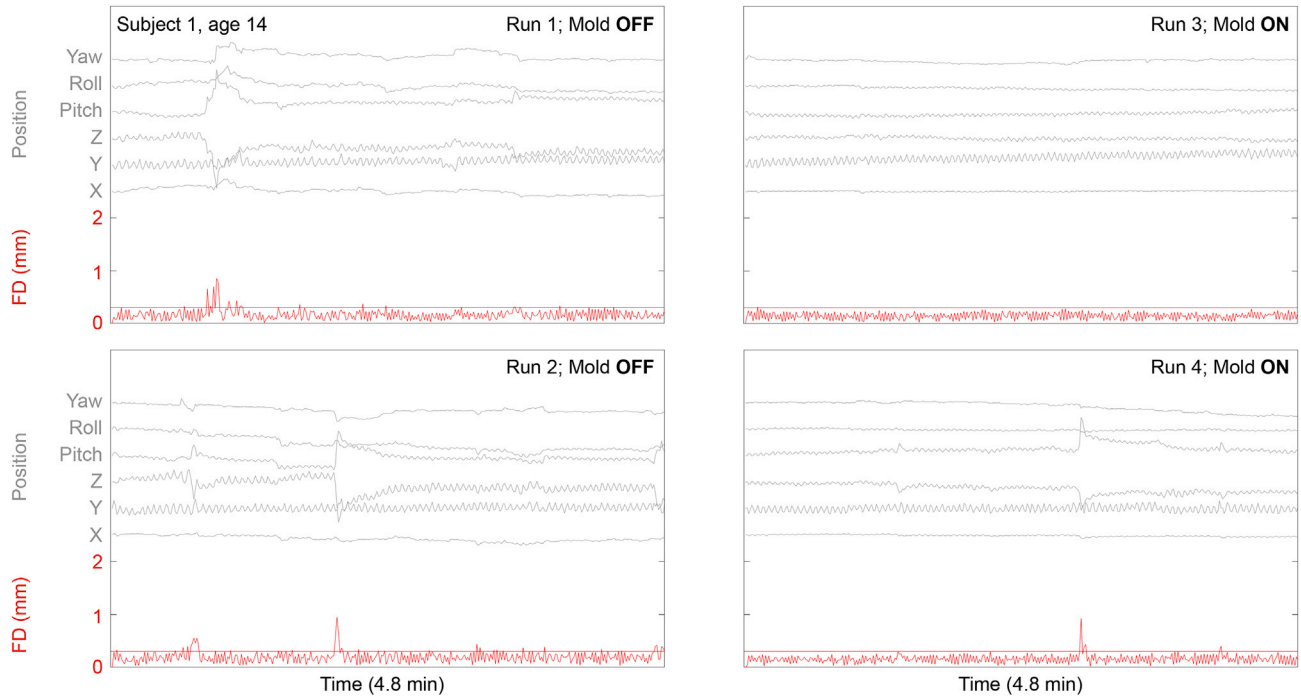


**Fig. 1.** : Position and motion estimates in the four runs of the first subject. The horizontal red line is set at FD = 0.30 mm. Position estimates show respiratory motion prominent in the Y, Z, and pitch traces, as expected (see Figure S2 for respiratory data). The continuous motion is attenuated with the mold on, and the prevalence of large motions is also reduced. This subject has an AABB run order (A = mold OFF, B = mold ON). See Figures S3-S5 for further examples in a 7 year old, a 17 year old, and a 28 year old. Such plots for all subjects are in the online movie.

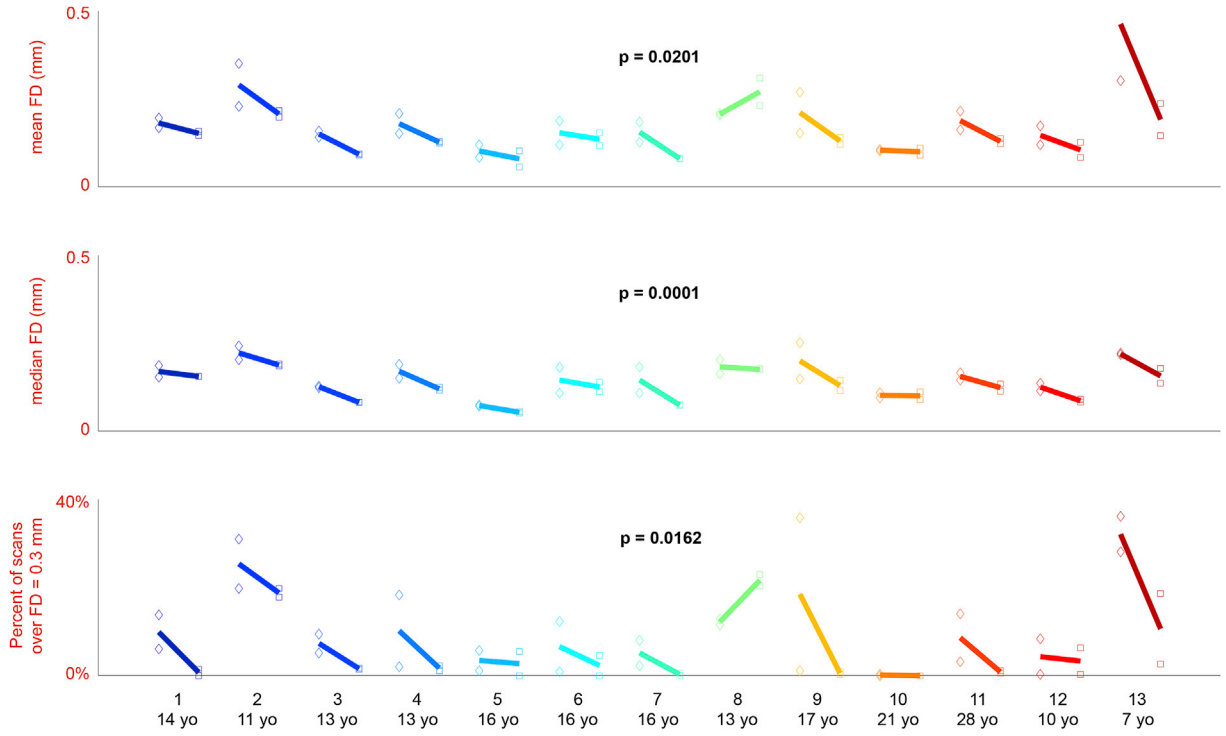


**Fig. 2.** Reduction in motion by head molds. For statistics of mean FD, median FD, and percent scan with motion over FD = 0.3 mm, values for each scan (diamonds = mold OFF; squares = mold ON) are shown for each subject (colors, with subject age at bottom). Lines show the change between mean values with mold OFF and ON. P values result from paired t-tests of mean values across the 13 subjects.

(in time) across the brain at each volume (Glasser et al., 2018; Power, 2017; Power et al., 2012, 2014; Smyser et al., 2010). DVARS is computed by differentiating an image by backwards differences in time, and then computing the root mean square across the brain (here, using the above whole-brain mask) at each volume. By convention, DVARS = 0 at the first volume. DVARS was calculated on fMRI images after transformation to the atlas space, and these DVARS values are treated in Fig. 4 in the same manner as the FD traces in Figs. 2 and 3.

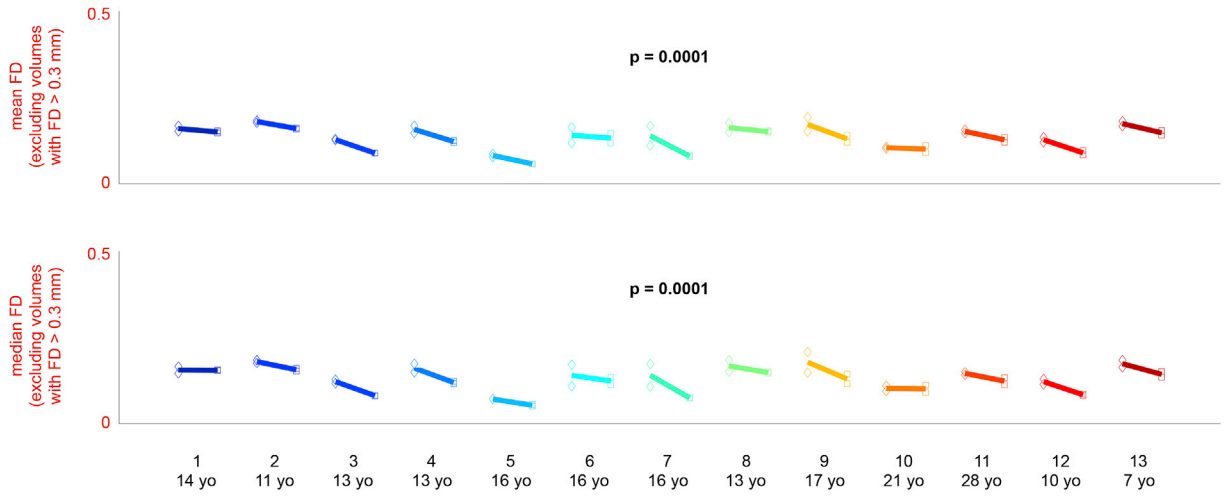


**Fig. 3.** Reduction in small motion by head molds. As for Fig. 2, but now only examining volumes with FD < 0.3 mm, to focus on the small, constant motions seen throughout a scan.

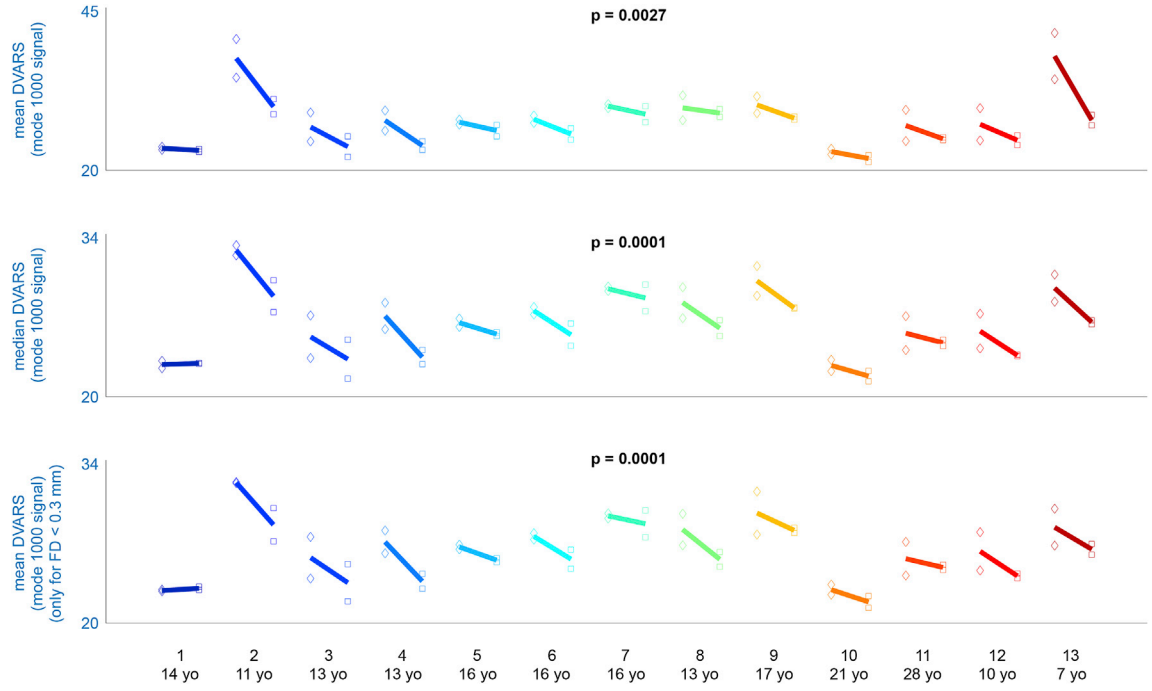


**Fig. 4.** Reduction in DVARS by head molds. As for Fig. 3, but for mean and median DVARS of the entire scan at top and middle, and for mean DVARS in only low-motion volumes at bottom. P values are from paired t-tests as before.

To assay signal covariance, a 264-region-of-interest (ROI) brain atlas was used (Power et al., 2011), in which ROIs were modeled as 10 mm diameter spheres; these ROIs are well-studied and have been used to characterize motion-related variance in numerous publications (Ciric et al., 2017; Power et al., 2012, 2014, 2017a, 2017b, 2018). In each run, signals at all ROIs were extracted, and the mean and linear trend terms were removed. No denoising was performed since the purpose of examining these signals is to measure noise-related properties.

To document the presence of distance-dependent artifact due to head motion, scrubbing analyses were performed in all subjects. These analyses are discussed in detail in (Power et al., 2015). In each run, a $264 \times 264$ Pearson correlation matrix followed by Fisher-Z transformation was constructed from the timeseries, using either all volumes or only volumes with FD < 0.3 mm (i.e., only low-motion volumes). The difference between these matrices was calculated, and the mean of these matrices is shown in Fig. 5, plotted as a function of the distance between the ROIs, yielding the well-documented pattern of distant-dependent changes in correlations when high-motion volumes are withheld from covariance calculations. An identical set of calculations was performed on a temporally shifted version of the temporal mask in each subject (moved a random fraction of the scan in a circular shift), to yield "random scrubbing" of the data, which yields no distance dependent changes in correlations, also shown in Fig. 5. This result establishes that motion artifact, and its distance-dependent properties, are specifically occurring during times of motion. Examples of the means of the "mold ON" and "mold OFF" patterns in several subjects are shown in Fig. 5, as are the averages of the mold ON and OFF conditions across subjects.

To show the difference in correlations seen in scans with mold ON versus mold OFF (as opposed to the difference between high- and low-motion volumes examined in scrubbing analyses), the within-subject

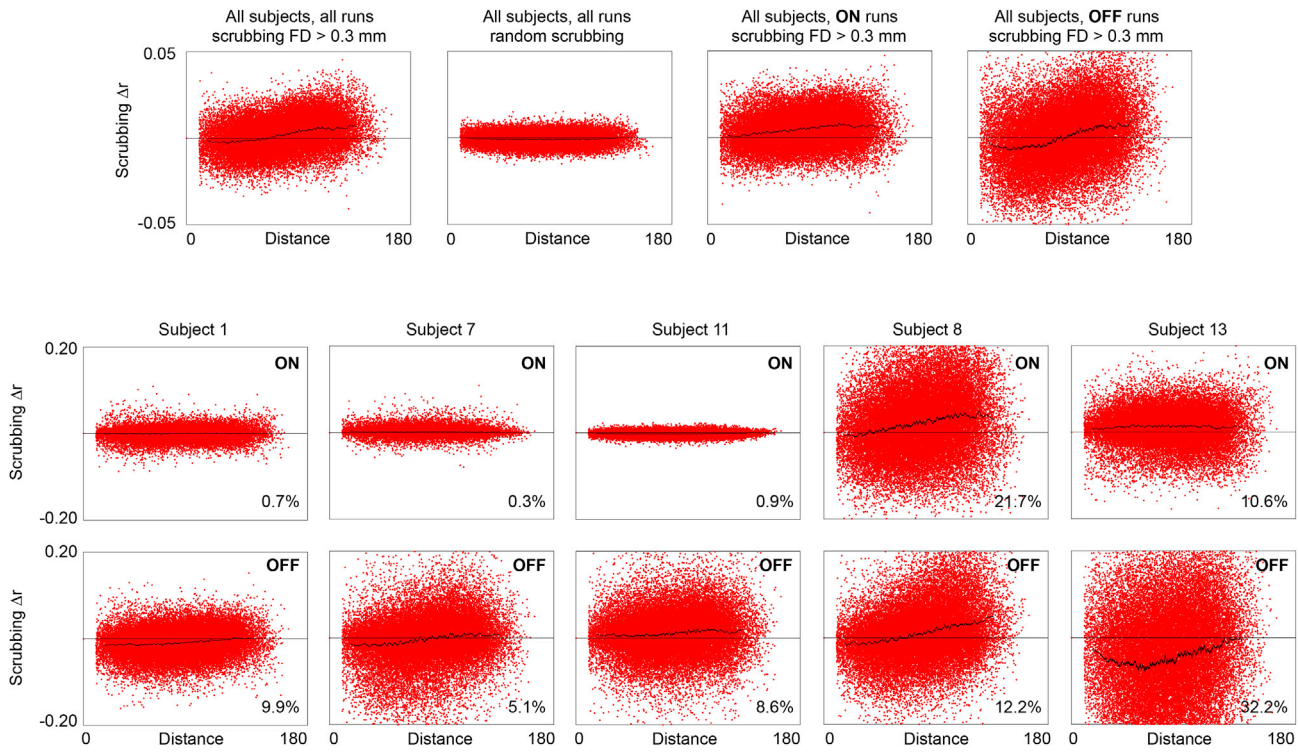


**Fig. 5.** Confirmation of distance-dependent artifact in high motion volumes. At top, a scrubbing analysis including all subjects and all runs, with scrubbing threshold of FD > 0.3 mm, showing distance-dependent artifact. For comparison, the effect of scrubbing identical numbers of volumes at random yields no distance-dependent effect. Scrubbing analyses of all mold ON and OFF runs show more distance-dependent artifact in the OFF runs, in part because there are more large motions (and associated artifacts) to censor (see Fig. 2). At bottom, individual scrubbing plots for ON and OFF scans; the inset percentages denote how much of the scan was censored. Subject 8 is the sole subject who moved more in the head mold, and considerable distance-dependent artifact is seen in both ON and OFF scans.

difference between mold ON and mold OFF correlation matrices was calculated and plotted over distance, as shown in the top of Fig. 6. Mean values of these within-subject difference matrices over all subjects are shown at the bottom of Fig. 6, both for all volumes (left), and for only low-motion volumes (right). These plots yield a pattern congruent with the scrubbing analyses: scans with molds ON have lower nearby correlations and higher distant correlations. To statistically assess these patterns, as in (Power et al., 2018), smoothing curves were obtained via a 1000-point moving window, and the difference between smoothing curve values at 100 mm and 35 mm was calculated (to index distance-dependent artifact). The actual difference was compared to the differences seen across 10,000 permutations of mold ON/OFF labels, yielding the statistics seen in Fig. 6.

When making Figures, simply for readability, Fisher-Z-transformed correlations were re-transformed to Pearson correlations.

## 3. Results

### 3.1. Motion assessment

13 subjects completed scanning and underwent analysis. To illustrate the data of interest, Fig. 1 shows head position and head motion (FD) estimates in our first subject. In gray are the 6 head position traces from the realignment procedure. Note that periodic motion (zig-zags) at a respiratory frequency (approximately 0.30 Hz) occur most prominently in the Y (anterior-posterior), Z (superior-inferior) and pitch (head nod) directions, as would be expected from the head flexing about the neck and pivoting on the occiput from breathing. Figure S2 confirms that these motions are due to breathing by showing paired motion and respiratory traces from run 1, which have the same peak frequencies (0.29 Hz). The red FD trace in Fig. 1 shows head motion, with both constant motion from the respiratory breathing and occasional larger motions apparent.

In this 14-year-old subject, an AABB run order was used (A = mold OFF, B = mold ON). Visually, in the OFF scans at the left of the figure, there are more frequent large motions (e.g., over the red line of FD = 0.3 mm), and the amplitude of the smaller constant motions is higher, closer to the horizontal red line. With the mold on, motion is attenuated, but it is not eliminated. Similar visual impressions arise in other subjects (Figures S3-S5 show data from a 7-year-old, a 17-year-old, and a 28-year-old; plots for all subjects are in an online movie[1]). The threshold of FD = 0.3 mm shown by the red line was chosen by plotting a histogram of all FD values in all subjects and choosing a threshold well above the majority of FD values (Figure S6).

To quantify effects of mold ON versus mold OFF across subjects, 3 statistics were calculated in each run: mean FD, median FD, and fraction of the scan over the threshold of FD = 0.3 mm. The values of these statistics are shown for each subject in Fig. 2 (diamonds = mold OFF, squares = mold ON, colors are subjects). For each subject and for each statistic, the means of the two ON and two OFF runs, respectively, were calculated, and these are shown by the bold lines of Fig. 2. Paired t-tests of the ON versus OFF values yielded the p values shown in the Figure. Having the mold on yielded lower mean FD in 12 of 13 subjects, lower median FD in 12 of 13 subjects, and lower fractions of the scan with supra-threshold motion in 12 of 13 subjects, all significant reductions by the paired *t*-test (see Figure). From these statistics it is evident that large motions are less frequent with the head mold on. To better characterize motion during the majority of the scan without supra-threshold motion, mean and median FD values were re-calculated in only volumes with FD < 0.3 mm. These statistics are shown in Fig. 3 and indicate that head molds reduced small, constant motion seen throughout the scan in every

[1] https://www.jonathanpower.net/2018-head-molds.html; a movie illustrating position and motion estimates for all subjects is available, as is a movie of "grayplots" of the same subjects, along with respective scrubbing analyses.

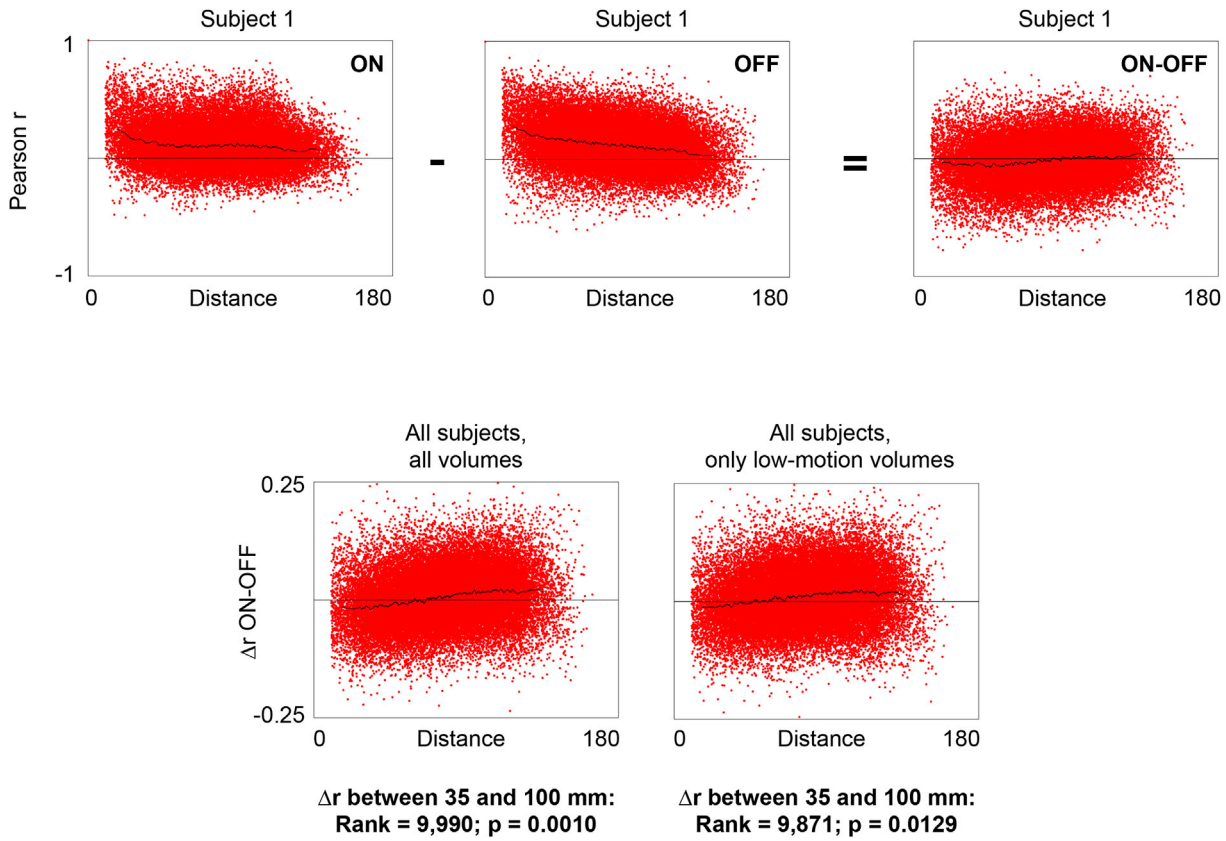


**Fig. 6.** Differences in correlations over distance with head molds ON versus OFF. At top, in a single subject, correlations are shown in the mold ON and mold OFF conditions, and the difference is also shown. Average values of the difference over all subjects are shown at bottom, both for all volumes (left, including high-motion volumes) and only lowmotion volumes (right, excluding volumes with FD > 0.3 mm). In mold ON scans, short-distance correlations are weaker, and long-distance correlations are stronger, relative to mold OFF scans. The significance of these distance-dependent changes was determined by measuring the Δr of the real smoothing curve between 35 mm and 100 mm distances, compared to the Δr of smoothing curves derived from 10,000 random permutations of ON/OFF labels as in (Power et al., 2018).

subject, and these reductions were significant.

In summary, across subjects, the fraction of a scan with FD over 0.3 mm dropped by 6% on average, a 60% reduction; mean FD dropped by 0.05 mm, a 25% reduction; and median FD dropped by 0.03 mm, a 20% reduction. In low-motion volumes only, mean FD dropped by 20% as did median FD. These results indicate not only a gain in usable volumes (and potentially degrees of freedom in the data) but also likely a gain in quality throughout the scan due to lower sub-threshold motion throughout the scan.

When individual position parameters are examined, both in terms of absolute displacement from the start of the run, and in terms of absolute motion from volume to volume, patterns emerge in how the head molds constrain head motion (see Figure S7 for all statistics). Mean, median, and standard deviation measures are reduced for absolute displacement of the head in all 6 parameters, especially in the X ($p = 0.0173$; $p = 0.0123$, respectively for median and standard deviation, using paired t-tests), pitch ($p = 0.0425$; $p = 0.0365$), roll ($p = 0.0221$; $p = 0.0350$), and yaw ($p = 0.0743$; $p = 0.0732$) directions. Absolute motion is also reduced in all parameters, most significantly in X ($p = 0.0027$; $p = 0.0361$), Z ($p = 0.0002$; $p = 0.0899$), pitch ($p = 0.0077$; $p = 0.1423$), roll ($p = 0.0121$; 0.1255), and yaw ($p = 0.0368$; $p = 0.1543$) directions. When only volumes with small motion (i.e., FD < 0.3 mm) are considered, effects remain significant in the same pattern: X ($p = 0.0079$; $p = 0.0000$), Z ($p = 0.0002$; $p = 0.0000$), pitch ($p = 0.0071$; $p = 0.0018$), roll ($p = 0.0153$; $p = 0.0684$), and yaw ($p = 0.1232$; $p = 0.1204$). Only in the Y direction do displacement and motion reductions fail to achieve even trend-level significance. Thus, the actions of the head mold are to most strongly constrain all rotations and movement in the left-right and superior-inferior directions. This pattern is sensible in light of the fact that the head is already resting (i.e., constrained) in an anterior-posterior direction due to gravity and the supine positioning of the head. There was no discernible effect of the molds on the directionality of drifts in head position (Figure S8).

Though we have no expectation that head molds versus foam padding would alter respiratory phenomena, given that some motion is related to periodic respiration (Figure S2), the data were examined for any influence of mold ON and OFF conditions on respiratory traces. Due to acquisition errors only four subjects had full complements of respiratory records, but, in these four subjects, respiratory rates are similar within subjects over runs, and there was no evidence of any systematic effect of the molds (Figure S9).

### 3.2. *Signal assessment*

The deleterious effects of motion on fMRI image quality are well-documented, as is motion's spatially patterned influence on signal covariance (Baum et al., 2018; Friston et al., 1996; Power et al., 2012, 2015, 2017a; Satterthwaite et al., 2012; Van Dijk et al., 2012; Yan et al., 2013). The reductions in motion in the mold ON condition ought to yield scans with better quality measures, less spatially focal artifact, and thus less distance-dependent covariance due to motion artifact. The next analyses assess these expectations.

DVARS is a data quality measure that indexes in a scan the rate of signal change over time (Power et al., 2012; Smyser et al., 2010). DVARS generally scales with subject motion (Power et al., 2014), and if mold ON scans have reduced motion, then DVARS measures should be lower. In

Fig. 4, DVARS measures in each run of each subject were treated in the same manner as the motion traces in Figs. 2 and 3, yielding consistent reductions of DVARS in mold ON scans no matter whether measured as mean over runs (top row, Fig. 4), median over runs (middle row, Fig. 4), or whether calculated only in low-motion volumes (mean is shown in the bottom row). Broadly, these findings indicate improved image quality in the "mold ON" condition, and that these improvements occur throughout the entire scan.

In general, as expected, FD effects scale with DVARS effects. The exception is Subject 8, which displays higher mean FD but lower DVARS with molds ON. The feature driving high mean FD in this subject is that there were a substantial number of extremely high FD values (near 4 in many instances) in one of the ON scans, visible in the online movie, whereas the median FD values were equivalent and the low-motion FD values were lower (as in all the subjects). The fact that DVARS went down is due to the highest FD values not scaling linearly with the corresponding DVARS values. FD and DVARS formally measure different things and were never intended to be regarded as equivalent, though they are in practice often closely related.

To assay the existence of spatially focal motion artifacts, which lead to distance-dependent covariance changes (i.e., increased local correlations and decreased distant correlations), scrubbing analyses were performed (Power et al., 2012, 2015). Pairwise correlations between 264 ROIs were calculated using all volumes of each run, and then using only volumes with FD $< 0.3$ mm in each run, and the difference was calculated. The average within-run difference was calculated over all subjects and runs, and these values are plotted as a function of the distance between ROIs in the top left panel of Fig. 5. In this analysis, withholding high-motion volumes decreases short-distance correlations and increases long-distance correlations, the familiar pattern of distance-dependent artifact caused by motion. This pattern is specific to the times exhibiting motion, for if the temporal mask used to censor high-motion volumes is randomly shifted in time, the distance-dependent effect is lost (the "random scrubbing" analysis). At upper right, analyses in mold ON and mold OFF runs demonstrate greater distance-dependent changes in the mold OFF condition, which is sensible given that there are more supra-threshold motions in this condition (Fig. 2). Scrubbing analyses are also shown for several individual subjects under mold ON and OFF conditions, again illustrating greater motion artifact in mold OFF scans (Subject 8, the sole subject who moved more with the mold ON, is shown, and distance-dependent artifact is prominent in both the ON and OFF condition). These analyses collectively demonstrate that distance-dependent motion artifact is present, that distance-dependent motion artifact is specific to periods of supra-threshold motion, and that motion artifact has a greater influence on covariance in the mold OFF condition.

To complement the scrubbing assays, the within-subject change in correlations between the mold ON and OFF conditions was also calculated and examined over distance, as shown at the top of Fig. 6 for a single subject. These analyses contrast the variance seen in entire scans, rather than the variance seen in low- and high-motion volumes. The bottom row summarizes the effect across subjects. Across subjects, scans with the mold ON have lower short-distance correlations and higher long-distance correlations, consistent with reduced motion artifact. This effect is found when correlations are calculated over all volumes, and, importantly, it is also found when high-motion volumes (i.e., FD $> 0.3$ mm) are excluded. This latter finding cannot be established via scrubbing analyses, since only sub-threshold volumes are contributing to correlations. To determine the significance of these distance-dependent patterns, the labels of ON and OFF runs were permuted randomly 10,000 times, and the change in correlation of the smoothing curves from 35 mm to 100 mm was calculated to index distance-dependent effects, as in (Power et al., 2018). In both analyses, the actual distance-dependent change in correlations is among the largest found amongst all permutations (and is thus significant). Because we are contrasting conditions in these analyses, it is conceivable, though we think it unlikely, that these effects could be due to the conditions themselves, i.e., neural differences due to psychological or physiological differences of having a mold on.

## 4. Discussion

Head motion is a known and much-discussed problem for fMRI scans (Caballero-Gaudes and Reynolds, 2017). Here we tried to prevent head motion from occurring by physically restraining the head in the head coil. In the first 13 subjects that we scanned with and without customized Styrofoam head molds, we found that head molds decreased head rotation and translation, reduced the fraction of a scan with large motions, and reduced the size of the small, constant motions seen throughout a scan. These effects were consistent across subjects spanning 7–28 years old, most of whom were adolescents. The reductions in motion should translate into generally increased data quality and decreased fractions of scans that are severely compromised by motion artifact.

When we examined the fMRI signals of these scans, we found that using head molds tended to yield scans with improved quality indices. Though motion artifact was still present in the scans, it was attenuated relative to scans obtained with foam padding in the head coil. Wearing the head mold reduced the proportion of a scan with large supra-threshold motions and thus the amount of motion artifact detected in scrubbing analyses. And, interestingly, it appeared that the reduction in sub-threshold, constant motion throughout a scan manifested as reduced distance-dependent correlations in the mold ON condition, since that effect was found even when excluding high-motion volumes from correlation calculations (Fig. 6). It should be noted that even though distance-dependent effects can be "unmasked" by particular post-processing procedures (e.g., (Power et al., 2018; Satterthwaite et al., 2013)), the distance-dependent artifact is inherent to the unprocessed data (Power et al., 2017a), and the reduction of distance-dependent artifact seen with the head molds follows as a consequence of reduced motion in the mold ON condition.

The chief drawbacks of the head molds are the production cost, the delay between scanning a subject's head and receiving a head mold, and the fact that the head molds can interfere with instrumentation around the head. The cost of molds will likely fluctuate in the future according to demand, competition, business model, and refinements of production processes, but, during the period of testing here, the cost was approximately $100–150 per mold. The drawback concerning instrumentation can be ameliorated by modifying the head mold as needed, either during production or post-hoc (since the Styrofoam can be altered by hand with a knife or Dremel tool). The chief benefit of the head mold approach, other than the reduction of motion, is that it requires no alteration in the behavior or "task set" of the participant (in contrast to approaches that provide feedback to reduce head motion).

3-D printing is typically done using hard polymers, whereas we elected to pursue collaboration with a commercial company producing milled Styrofoam molds. This choice was partly for convenience, and partly due to suspicion that a softer material would be more comfortable for our subjects. We have not directly compared Styrofoam head molds to more rigid head molds. It is possible that harder molds would constrain motion to a greater extent than our relatively soft molds, however, they may also be less comfortable for participants and would be difficult to modify once produced. The present versions of our molds do not restrain the chin, and they are also sculpted to have little or no contact with the nose and cheeks, as many subjects disliked those sensations. Having contact at these locations may more fully constrain the head and prevent motion to a greater extent.

When we first began using the head molds, we were in close contact with the company producing the head molds to suggest alterations to mold shapes, since these molds had not been used in pediatric populations, where the angle and size of the neck in the head coil is different than in adults. Several of our initial participants reported some discomfort, especially at the back of the head and the cheeks. Modifications to the molds were made, especially modification of the thickness of the

posterior part of the mold, and we have now used head molds with many children and adolescents, including children and adults with autism, without further report of discomfort or poor fits. We now routinely produce head molds for subjects in a variety of studies. In the one subject (#8 in Fig. 2) who had increased motion with the head mold, there was no report of discomfort and we have no particular explanation for why motion was higher with the mold on.

Readers may wonder whether certain kinds of subjects may have difficulties with the molds. Our clinical experience thus far is mainly with pediatric subjects, and both healthy control and clinical populations wear the molds without notable issues. In terms of whether certain hairstyles might complicate mold use, we use a swim cap while optically scanning the subject to compress hair to a similar extent that the actual mold will compress it. Although we have not scanned subjects with extremely voluminous hair, we have not found even "big" hair to be an obstacle to using the molds. A point worth noting is that when optically scanning subjects, hair should be lifted away from the neck to provide an accurate estimate of anatomy. One of our reviewers raised the possibility that certain subjects may be sensitive to overheating in the molds. None of our subjects reported sweating or feeling hot, though common sense would lead one to suspect that faces are hotter with reduced convective currents and the insulating effects of the Styrofoam. Those of us on the investigative team who have worn the molds did not note effects of heat, and the dozens of pediatric and young adult subjects we have scanned with molds also have not raised heat as an issue. However, older or other clinical populations might experience this effect.

In summary, our experience with customized Styrofoam head molds indicates that they reduce motion during fMRI scans, and that subjects find them comfortable to use (after the initial modifications noted above). In populations prone to movement, such as pediatric, elderly, and clinical groups, these molds may increase the efficiency of scanning by decreasing the fraction of a scan compromised by substantial movement, and may increase the quality of a scan by generally dampening movement throughout a scan. We report here on task-free resting state scans, but the molds should be useful for all kinds of MRI scanning.

## Conflicts of interest

The authors declare no conflicts of interest with respect to this report.

## Acknowledgments

We thank James Gao and the Caseforge company for their support and assistance in modifying head molds for our pediatric subjects. This work was supported by Simons Foundation Grant 528440, the Mortimer D. Sackler, M.D. family, and a gift from Robert Shapiro.

## Appendix A. Supplementary data

Supplementary data to this article can be found online at https://doi.org/10.1016/j.neuroimage.2019.01.016.

## References

Barch, D.M., Sabb, F.W., Carter, C.S., Braver, T.S., Noll, D.C., Cohen, J.D., 1999. Overt verbal responding during fMRI scanning: empirical investigations of problems and potential solutions. Neuroimage 10, 642–657.

Barnea-Goraly, N., Weinzimer, S.A., Ruedy, K.J., Mauras, N., Beck, R.W., Marzelli, M.J., Mazaika, P.K., Aye, T., White, N.H., Tsalikian, E., Fox, L., Kollman, C., Cheng, P., Reiss, A.L., Diabetes Research in Children, N., 2014. High success rates of sedation-free brain MRI scanning in young children using simple subject preparation protocols with and without a commercial mock scanner–the Diabetes Research in Children Network (DirecNet) experience. Pediatr. Radiol. 44, 181–186.

Baum, G.L., Roalf, D.R., Cook, P.A., Ciric, R., Rosen, A.F.G., Xia, C., Elliott, M.A., Ruparel, K., Verma, R., Tunc, B., Gur, R.C., Gur, R.E., Bassett, D.S., Satterthwaite, T.D., 2018. The impact of in-scanner head motion on structural connectivity derived from diffusion MRI. Neuroimage 173, 275–286.

Bright, M.G., Murphy, K., 2013. Removing motion and physiological artifacts from intrinsic BOLD fluctuations using short echo data. Neuroimage 64, 526–537.

Bullmore, E.T., Brammer, M.J., Rabe-Hesketh, S., Curtis, V.A., Morris, R.G., Williams, S.C., Sharma, T., McGuire, P.K., 1999. Methods for diagnosis and treatment of stimulus-correlated motion in generic brain activation studies using fMRI. Hum. Brain Mapp. 7, 38–48.

Caballero-Gaudes, C., Reynolds, R.C., 2017. Methods for cleaning the BOLD fMRI signal. Neuroimage 154, 128–149.

Casey, B.J., Cannonier, T., Conley, M.I., Cohen, A.O., Barch, D.M., Heitzeg, M.M., Soules, M.E., Teslovich, T., Dellarco, D.V., Garavan, H., Orr, C.A., Wager, T.D., Banich, M.T., Speer, N.K., Sutherland, M.T., Riedel, M.C., Dick, A.S., Bjork, J.M., Thomas, K.M., Chaarani, B., Mejia, M.H., Hagler Jr., D.J., Daniela Cornejo, M., Sicat, C.S., Harms, M.P., Dosenbach, N.U.F., Rosenberg, M., Earl, E., Bartsch, H., Watts, R., Polimeni, J.R., Kuperman, J.M., Fair, D.A., Dale, A.M., Workgroup, A.I.A., 2018. The adolescent brain cognitive development (ABCD) study: imaging acquisition across 21 sites. Dev Cogn Neurosci 32, 43–54.

Ciric, R., Wolf, D.H., Power, J.D., Roalf, D.R., Baum, G.L., Ruparel, K., Shinohara, R.T., Elliott, M.A., Eickhoff, S.B., Davatzikos, C., Gur, R.C., Gur, R.E., Bassett, D.S., Satterthwaite, T.D., 2017. Benchmarking of participant-level confound regression strategies for the control of motion artifact in studies of functional connectivity. Neuroimage 154, 174–187.

de Bie, H.M., Boersma, M., Wattjes, M.P., Adriaanse, S., Vermeulen, R.J., Oostrom, K.J., Huisman, J., Veltman, D.J., Delemarre-Van de Waal, H.A., 2010. Preparing children with a mock scanner training protocol results in high quality structural and functional MRI scans. Eur. J. Pediatr. 169, 1079–1085.

Deen, B., Richardson, H., Dilks, D.D., Takahashi, A., Keil, B., Wald, L.L., Kanwisher, N., Saxe, R., 2017. Organization of high-level visual cortex in human infants. Nat. Commun. 8, 13995.

Dosenbach, N.U.F., Koller, J.M., Earl, E.A., Miranda-Dominguez, O., Klein, R.L., Van, A.N., Snyder, A.Z., Nagel, B.J., Nigg, J.T., Nguyen, A.L., Wesevich, V., Greene, D.J., Fair, D.A., 2017. Real-time motion analytics during brain MRI improve data quality and reduce costs. Neuroimage 161, 80–93.

Epstein, J.N., Casey, B.J., Tonev, S.T., Davidson, M., Reiss, A.L., Garrett, A., Hinshaw, S.P., Greenhill, L.L., Vitolo, A., Kotler, L.A., Jarrett, M.A., Spicer, J., 2007. Assessment and prevention of head motion during imaging of patients with attention deficit hyperactivity disorder. Psychiatr. Res. 155, 75–82.

Fair, D.A., Nigg, J.T., Iyer, S., Bathula, D., Mills, K.L., Dosenbach, N.U., Schlaggar, B.L., Mennes, M., Gutman, D., Bangaru, S., Buitelaar, J.K., Dickstein, D.P., Di Martino, A., Kennedy, D.N., Kelly, C., Luna, B., Schweitzer, J.B., Velanova, K., Wang, Y.F., Mostofsky, S., Castellanos, F.X., Milham, M.P., 2012. Distinct neural signatures detected for ADHD subtypes after controlling for micro-movements in resting state functional connectivity MRI data. Front. Syst. Neurosci. 6, 80.

Friston, K.J., Williams, S., Howard, R., Frackowiak, R.S., Turner, R., 1996. Movement-related effects in fMRI time-series. Magn. Reson. Med. 35, 346–355.

Glasser, M.F., Coalson, T.S., Bijsterbosch, J.D., Harrison, S.J., Harms, M.P., Anticevic, A., Van Essen, D.C., Smith, S.M., 2018. Using temporal ICA to selectively remove global noise while preserving global signal in functional MRI data. Neuroimage 181, 692–717.

Greene, D.J., Koller, J.M., Hampton, J.M., Wesevich, V., Van, A.N., Nguyen, A.L., Hoyt, C.R., McIntyre, L., Earl, E.A., Klein, R.L., Shimony, J.S., Petersen, S.E., Schlaggar, B.L., Fair, D.A., Dosenbach, N.U.F., 2018. Behavioral interventions for reducing head motion during MRI scans in children. Neuroimage 171, 234–245.

Kundu, P., Brenowitz, N.D., Voon, V., Worbe, Y., Vertes, P.E., Inati, S.J., Saad, Z.S., Bandettini, P.A., Bullmore, E.T., 2013. Integrated strategy for improving functional connectivity mapping using multiecho fMRI. Proc. Natl. Acad. Sci. U. S. A. 110, 16187–16192.

Nordahl, C.W., Mello, M., Shen, A.M., Shen, M.D., Vismara, L.A., Li, D., Harrington, K., Tanase, C., Goodlin-Jones, B., Rogers, S., Abbeduto, L., Amaral, D.G., 2016. Methods for acquiring MRI data in children with autism spectrum disorder and intellectual impairment without the use of sedation. J. Neurodev. Disord. 8, 20.

Patel, A.X., Kundu, P., Rubinov, M., Jones, P.S., Vertes, P.E., Ersche, K.D., Suckling, J., Bullmore, E.T., 2014. A wavelet method for modeling and despiking motion artifacts from resting-state fMRI time series. Neuroimage 95, 287–304.

Power, J.D., 2017. A simple but useful way to assess fMRI scan qualities. Neuroimage 154, 150–158.

Power, J.D., Barnes, K.A., Snyder, A.Z., Schlaggar, B.L., Petersen, S.E., 2012. Spurious but systematic correlations in functional connectivity MRI networks arise from subject motion. Neuroimage 59, 2142–2154.

Power, J.D., Cohen, A.L., Nelson, S.M., Wig, G.S., Barnes, K.A., Church, J.A., Vogel, A.C., Laumann, T.O., Miezin, F.M., Schlaggar, B.L., Petersen, S.E., 2011. Functional network organization of the human brain. Neuron 72, 665–678.

Power, J.D., Mitra, A., Laumann, T.O., Snyder, A.Z., Schlaggar, B.L., Petersen, S.E., 2014. Methods to detect, characterize, and remove motion artifact in resting state fMRI. Neuroimage 84, 320–341.

Power, J.D., Plitt, M., Gotts, S.J., Kundu, P., Voon, V., Bandettini, P.A., Martin, A., 2018. Ridding fMRI data of motion-related influences: removal of signals with distinct spatial and physical bases in multiecho data. Proc. Natl. Acad. Sci. U. S. A. 115, E2105–E2114.

Power, J.D., Plitt, M., Kundu, P., Bandettini, P.A., Martin, A., 2017a. Temporal interpolation alters motion in fMRI scans: magnitudes and consequences for artifact detection. PLoS One 12, e0182939.

Power, J.D., Plitt, M., Laumann, T.O., Martin, A., 2017b. Sources and implications of whole-brain fMRI signals in humans. Neuroimage 146, 609–625.

Power, J.D., Schlaggar, B.L., Petersen, S.E., 2015. Recent progress and outstanding issues in motion correction in resting state fMRI. Neuroimage 105, 536–551.

Pruim, R.H., Mennes, M., van Rooij, D., Llera, A., Buitelaar, J.K., Beckmann, C.F., 2015. ICA-AROMA: a robust ICA-based strategy for removing motion artifacts from fMRI data. Neuroimage 112, 267–277.

Salimi-Khorshidi, G., Douaud, G., Beckmann, C.F., Glasser, M.F., Griffanti, L., Smith, S.M., 2014. Automatic denoising of functional MRI data: combining independent component analysis and hierarchical fusion of classifiers. Neuroimage 90, 449–468.

Satterthwaite, T.D., Ciric, R., Roalf, D.R., Davatzikos, C., Bassett, D.S., Wolf, D.H., 2017 Nov 1. Motion artifact in studies of functional connectivity: characteristics and mitigation strategies. Hum. Brain Mapp. https://doi.org/10.1002/hbm.23665 [Epub ahead of print] Review. PMID: 29091315.

Satterthwaite, T.D., Elliott, M.A., Gerraty, R.T., Ruparel, K., Loughead, J., Calkins, M.E., Eickhoff, S.B., Hakonarson, H., Gur, R.C., Gur, R.E., Wolf, D.H., 2013. An improved framework for confound regression and filtering for control of motion artifact in the preprocessing of resting-state functional connectivity data. Neuroimage 64, 240–256.

Satterthwaite, T.D., Wolf, D.H., Loughead, J., Ruparel, K., Elliott, M.A., Hakonarson, H., Gur, R.C., Gur, R.E., 2012. Impact of in-scanner head motion on multiple measures of functional connectivity: relevance for studies of neurodevelopment in youth. Neuroimage 60, 623–632.

Savalia, N.K., Agres, P.F., Chan, M.Y., Feczko, E.J., Kennedy, K.M., Wig, G.S., 2017. Motion-related artifacts in structural brain images revealed with independent estimates of in-scanner head motion. Hum. Brain Mapp. 38, 472–492.

Smyser, C.D., Inder, T.E., Shimony, J.S., Hill, J.E., Degnan, A.J., Snyder, A.Z., Neil, J.J., 2010. Longitudinal analysis of neural network development in preterm infants. Cerebr. Cortex 20, 2852–2862.

Van Dijk, K.R., Sabuncu, M.R., Buckner, R.L., 2012. The influence of head motion on intrinsic functional connectivity MRI. Neuroimage 59, 431–438.

Yan, C.G., Cheung, B., Kelly, C., Colcombe, S., Craddock, R.C., Di Martino, A., Li, Q., Zuo, X.N., Castellanos, F.X., Milham, M.P., 2013. A comprehensive assessment of regional variation in the impact of head micromovements on functional connectomics. Neuroimage 76, 183–201.

Zaitsev, M., Akin, B., LeVan, P., Knowles, B.R., 2017. Prospective motion correction in functional MRI. Neuroimage 154, 33–42.